JOURNAL OF MATERIALS SCIENCE 19 (1984) 1007–1021

Effect of cold working and ageing treatment on ductility of an Al–6.0% Zn–2.6% Mg alloy at 4.2 to 293 K

T. KAWABATA, H. SUENAGA, O. IZUMI
The Research Institute for Iron, Steel and Other Metals, Tohoku University, Sendai 980, Japan

The effect of cold-working and ageing (CA) treatment on the ductility of an Al–Zn–Mg alloy was investigated at temperatures from 4.2 to 293 K. The ductility was improved by the CA treatment at 4.2, 77, 196 and 293 K. It was found that both the fracture strain and the reduction of area vary linearly with the area fraction of transgranular fracture. The improvement of ductility was thought to be due to the shape of the grain boundary, the formation of a subboundary and the scattering precipitate size in grains by which both the ledge- and the dimple-formation type intergranular fractures are difficult to occur. The increase of intergranular fracture with decreasing temperature is attributed to the increase of the difference between flow stresses in PFZ and in the matrix, the brittleness of grain boundary precipitates themselves, and the incoherent interface between grain boundary precipitates and the matrix. An intergranular fracture mechanism in the CA specimen is proposed.

1. Introduction

The ductility of high strength Al–Zn–Mg alloys is usually poor because of the occurrence of intergranular fracture. On the morphology of the intergranular fracture in the alloys, a dimple- and a ledge-formation type have been reported [1–6]. Based on the concept that the dimple-formation type is ductile fracture in the precipitate-free-zone (PFZ) existing along grain boundaries, the ductility has been discussed in relation to the width of PFZ and the size and density of grain boundary precipitates [2]. The ledge-type intergranular fracture is said to occur due to the separation of grain boundaries caused by the stress concentration of piled up dislocations [6].

The ductility of Al–Zn–Mg alloys decreases with decreasing testing temperature because the intergranular fracture is more favourable at lower temperature [7–9].

Thermomechanical treatments, i.e. combinations of working and ageing treatment raise the strength of Al–Zn–Mg base alloys [10–15]. On the effect of the thermomechanical treatment on ductility, both the cases of ductility to increase and to decrease have been reported [10–16].

Recently Uno and Baba [16] have shown that the ductility is increased by a thermomechanical treatment, i.e. by cold-working and artificial ageing after solution treatment (CA treatment) in a high purity Al–Zn–Mg ternary alloy. They suggested that the increase of ductility is caused by restraining the coarsening of grain boundary precipitates and the formation of PFZ, and additionally by coarsening precipitates in grains.

The purpose of the present work is to study the effect of the CA treatment on ductility of an Al–6.0% Zn–2.6% Mg alloy at 4.2–293 K and to discuss the mechanism of ductility improvement due to the CA treatment in relation to two types of intergranular fracture.

2. Experimental procedures

The chemical composition of specimens was zinc: 6.0, magnesium: 2.6 and iron, silicon, copper <0.015 mass%, respectively, remainder: aluminium. After hot-worked at 670 K the material was

0022–2461/84 $03.00 + .12

solution treated at 733 K for 7.2 ksec, quenched into iced water and cold-worked to 50% reduction, then immediately aged at 393 K for 72 ksec. Unnotched specimens with the gauge portion of 3 mm in diameter and 30 mm in length were made by machining and aged further at 393 K for 14.4 ksec before testing to remove the influence of the worked zone (the CA specimens). For comparison, the specimens which were similarly heat treated to the CA specimens but not cold worked (the A specimens) were also tested. Tensile tests were performed using an Instron type testing machine at the strain rate of 1.2×10^{-3} sec^{-1} and at 293, 196, 77, and 4.2 K. An optical and a transmission electron microscope (JEM-200B) were used for structural observations. Fracture surfaces were observed using a scanning electron microscope (JSM-T20) by a stereographic method.

3. Results

3.1. Structural observations of undeformed specimen

Figs. 1a and b exhibit optical micrographs representing a transverse and a longitudinal section of the undeformed CA specimen, respectively. Grains are elongated by the cold working before ageing treatment and a large number of subboundaries are observable in the grains. Figs. 1c and d show a transverse and a longitudinal section of the undeformed A specimen in which grains are equiaxed and no subboundary is observable. Figs. 2a to c are transmission electron micrographs observed at high magnification showing subboundaries (arrow SB) and grain boundaries (arrow GB) in the undeformed CA specimen. Slightly larger precipitates than those in grains are formed on subboundaries. Various sizes of grain boundary precipitates are observable which would be formed dependent upon the structure of the grain boundary [17]. Fig. 2b is an example of a micrograph in which large grain boundary precipitates and PFZ are partly observable. Fig. 2c is another example of a grain boundary with small precipitates as if PFZ is hardly formed. In the matrix a large number of dislocations remain even after the ageing treatment as shown in Fig. 2c. It was difficult to make clear the contrast of dislocations (arrow D) because the contrast is duplicated and confused with that of precipitates. Three kinds of precipitates are seen in the matrix, i.e. the first are the precipitates with an ellipsoidal shape whose sizes are nearly equal to those on the subboundaries; the second is also

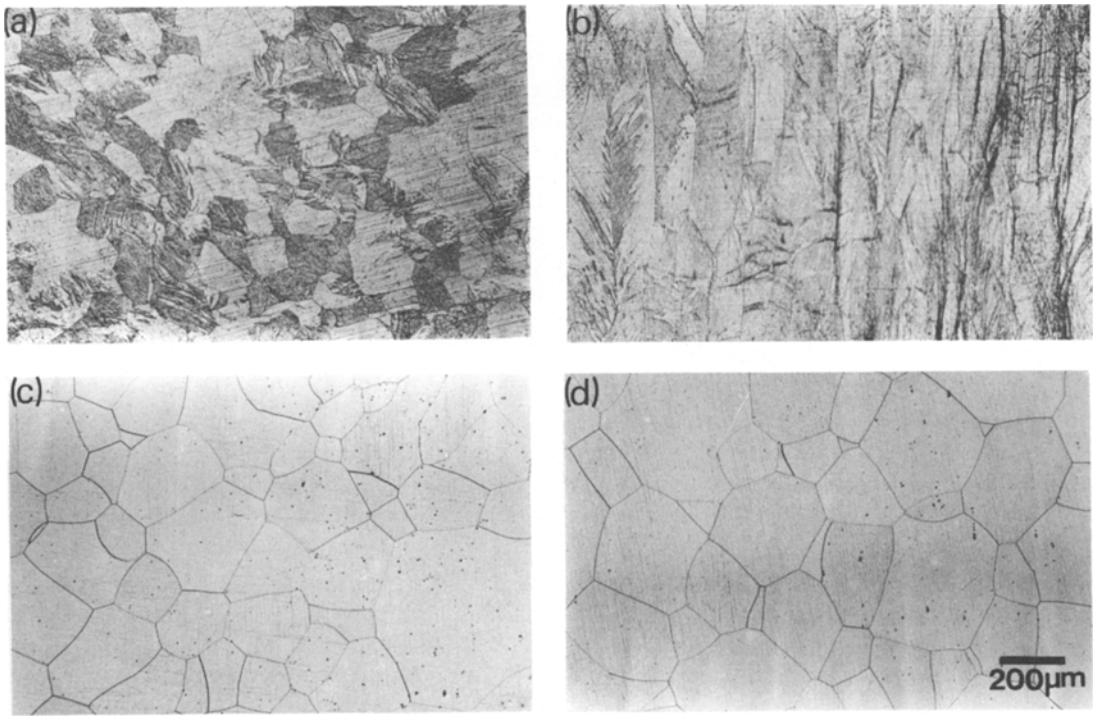

Figure 1 Optical micrographs showing the transverse ((a) and (c)) and the longitudinal sections ((b) and (d)) of the CA ((a) and (b)) and the A specimens ((c) and (d)) undeformed.

ellipsoidal precipitate but smaller than the first; and the third are large needle-like precipitates. It is characteristic that grain boundaries run in a zigzag way (Figs. 2b and c). Table I represents the results of structural observations on the CA and the A specimens by an optical and a transmission electron microscope. Various sizes of grain boundary precipitates are observable so that mean sizes of precipitate on three typical grain boundaries are exhibited. The mean width and the width distribution of PFZ are obtained by measuring at a given interval along grain boundaries. On calculating the mean width of PFZ in the CA specimen, the grain boundaries on which PFZ is hardly observable (e.g. Fig. 2c) are omitted.

3.2. Mechanical properties

The mechanical properties are shown in Fig. 3. In the CA specimens the yield stress, $\sigma_{0.2}$, the ultimate tensile stress, σ_{uts} and the fracture stress, σ_f, increase with decreasing temperature. However, the A specimens fractured at a small strain ($\sim 0.2\%$) at 196 K and within an elastic range at 77 K because of the remarkable brittleness. There-

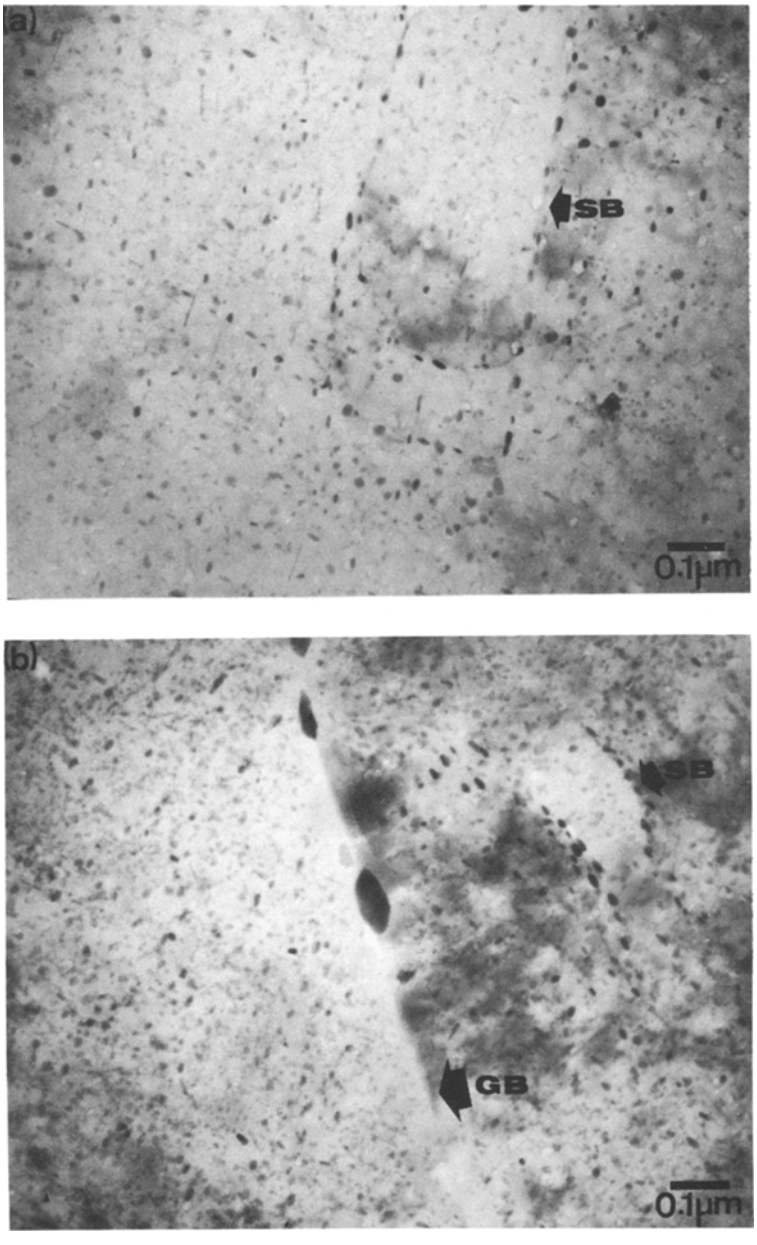

Figure 2 Transmission electron micrographs of the CA specimen showing subboundaries (a), a grain boundary with large precipitates and PFZ (b), and a grain boundary on which PFZ is hardly observable with small precipitates (c). A large number of dislocations remain even after ageing treatment (c). The arrows SB, GB and D show the subboundary, grain boundary and dislocation, respectively.

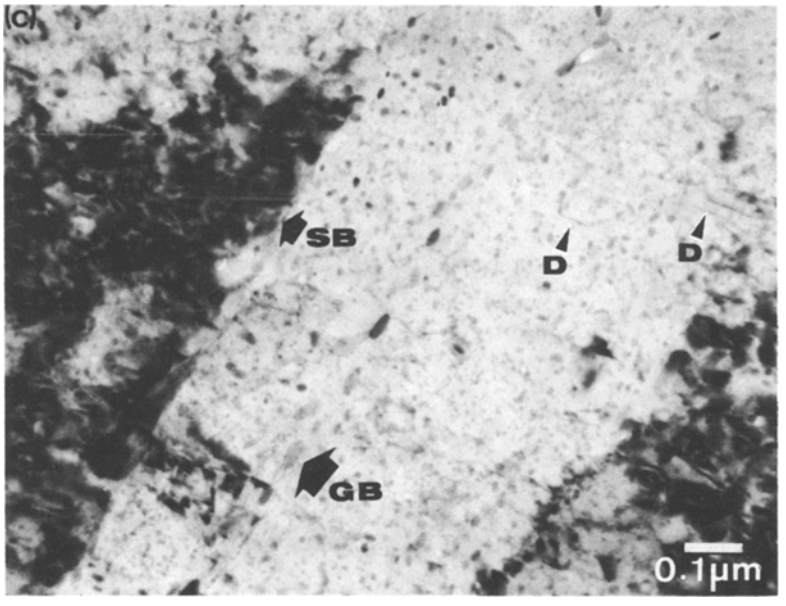

Figure 2 Continued.

fore σ_f of the A specimen seems apparently to decrease at 77 K. A notable difference between the CA and the A specimen is seen in the reduction of area (RA). At room temperature the values of RA in the CA and the A specimens are 45.5 and 12.1%, respectively, and both decrease with decreasing temperature. The values of RA in the CA specimens are larger than those in the A specimens, also at cryogenic temperatures. The results of mechanical properties are given in Table II.

3.3. Optical microstructure of the surface in a deformed specimen

Fig. 4 shows optical micrographs of the surface near the fracture portion of the CA (a) and the A specimen (b) deformed at 196 K. At all testing temperatures the coarse slip bands are formed in the A specimens. While, the CA specimens deform uniformly and no coarse slip band is observable.

3.4. Relations of the reduction of area and the fracture strain against the area fraction of intergranular fracture

Fig. 5 shows scanning electron micrographs of a fracture surface in the CA ((a) and (b)) and the A specimens ((c) and (d)) observed at low magnification and tested at 293 K ((a) and (c)), and 4.2 K ((b) and (d)). The CA specimens fracture transgranularly at 293 and 196 K but at 77 and 4.2 K the fracture changes to an intergranular one. In contrast the A specimen fractures intergranularly even at room temperature and the tendency is more pronounced with decreasing temperature.

TABLE I Parameters measured in the optical and the transmission electron micrographs

Heat treatment	Grain size (μm)	Size of grain boundary precipitates (μm)	Size of subboundary precipitates (μm)	Size of precipitates in matrix (μm)	Width of precipitate free zone (μm)
ST 733 K 7.2 ksec Cold working Ageing 393 K 86 ksec	Elongated 310 × 100	0.113 × 0.036 0.088 × 0.036 0.058 × 0.024	Ellipsoidal 0.019 × 0.0087	Ellipsoidal 0.021 × 0.013 Small ellipsoidal 0.010 × 0.0046 Needle 0.0665 × 0.0033	0.020 ~ 0.092
ST 733 K 7.2 ksec Ageing 393 K 86 ksec	Equiaxed 190	0.064 × 0.035		~ 0.002	0.063 ~ 0.0115 0.091*

Key: ST – solution treatment. * Average value.

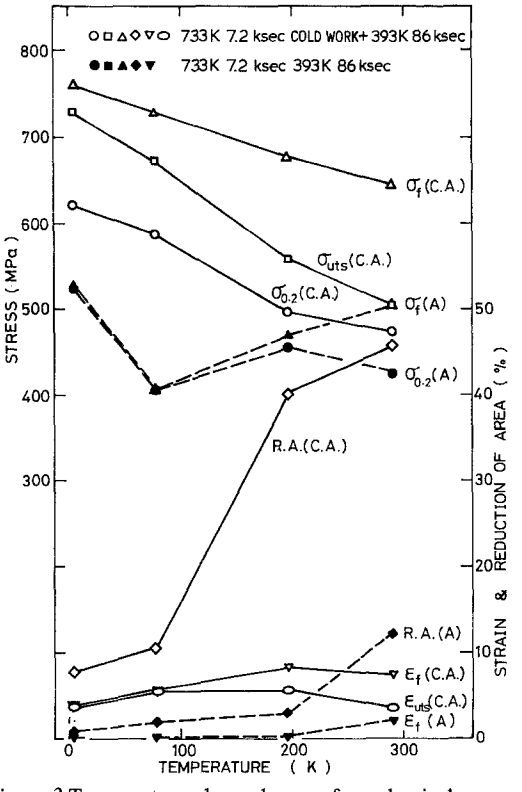

Figure 3 Temperature dependence of mechanical properties ($\sigma_{0.2}$, σ_{uts}, σ_f, ϵ_{uts}, ϵ_f, and RA) in the CA and the A specimens.

The area fractions of transgranular fracture (f_{TF}) are given in Table III. Not only at 293 K, but also at cryogenic temperatures, the values of f_{TF} in the CA specimens are larger than those of the A specimens. The fracture strain (ϵ_f) and RA against f_{TF} are plotted in Fig. 6. There are linear relationships in both ϵ_f against f_{TF} and RA against f_{TF}. That is, the facilitation of intergranular fracture correlates with the decrease of ϵ_f and RA.

3.5. Features of intergranular fracture surface

Fig. 7 shows scanning electron micrographs taken at high magnification showing intergranular fracture surfaces of the CA ((a) and (b)) and the A ((c) and (d)) specimens tested at 293 K ((a) and (c)), 196 K (d) and 4.2 K (b). At whole testing temperatures the intergranular fracture surfaces of the CA specimen consist of complicated and many linear patterns instead of dimples. In the A specimen, when tested at 293 K, fine dimples mingling with faint ledges are observable on the intergranular fracture surface. Below 196 K, many small steps of ledge and many traces of grain boundary precipitate are seen by observation at high magnification (× 10 000). But, dimples are hardly observable. The feature of fracture surfaces corresponds to the low ductility of the present alloy.

3.6. Optical microstructures of the longitudinal section

Fig. 8 shows optical micrographs of the longitudinal section near fracture surface in the CA ((a) and (b)) and the A specimens (c) tested at 196 K ((a) and (c)) and 77 K (b). At 293 and 196 K, after local necking, the CA specimens fracture in a cup and cone or a shear type. The cracking is also observable, as shown partly in Fig. 8a (arrow) along the grain boundaries parallel to the tensile axis far away from the fractured portion. Below 77 K the CA specimen tends to fracture intergranularly (Fig. 8b). In the A specimen, at 293 K, the fracture surface contains 20.4% transgranular fracture, and at 196, 77 and 4.2 K the intergranular fracture becomes notable. Figs. 9a and b

TABLE II Results of mechanical properties

Heat treatment	Testing temperature (K)	Reduction of area (%)	Strain to UTS (%)	Strain to fracture (%)	Yield stress, $\sigma_{0.2}$ (MPa)	Ultimate tensile stress, σ_{UTS} (MPa)	Fracture stress, σ_f (MPa)
ST 733 K 7.2 ksec	293	45.5	3.5	7.3	473.4	507.6	645.6
Cold working	196	40.2	5.5	8.3	496.9	559.3	677.0
Ageing 393 K 86 ksec	77	12.9	5.4	5.5	588.2	672.9	727.2
	4.2	7.9	3.6	3.6	623.3	727.5	760.1
	293	12.1	2.8	3.0	425.4	455.7	502.3
ST 733 K 7.2 ksec	196	2.8	(0.2)	0.2	456.2	(456.2)	469.3
Ageing 393 K 86 ksec	77	1.8	–	–	(398.7)	(398.7)	(405.8)
	4.2	0.9	0.1	0.1	–	(524.4)	(529.1)

Key: ST – solution treatment. ( ) – The value when the specimen fractured at the linear increasing portion in the load–elongation curve.

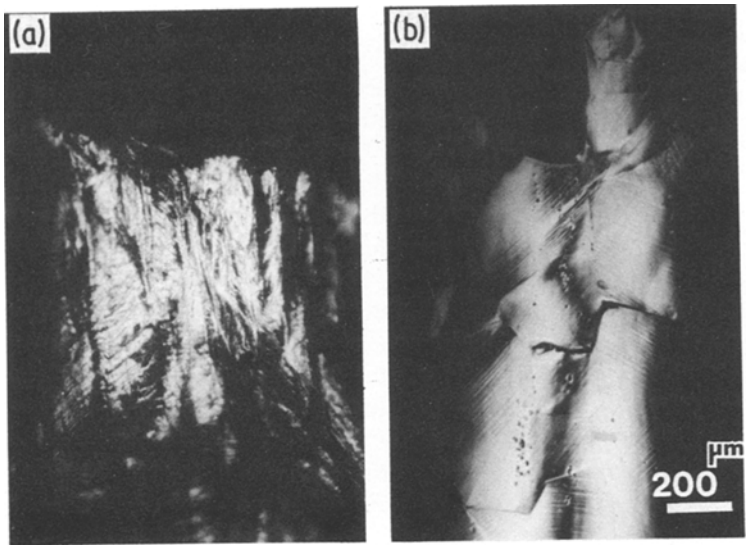

Figure 4 Optical micrographs showing surfaces of the CA (a), and the A specimen (b), tested at 196 K.

are optical micrographs showing cracks formed at grain boundaries in the uniformly deformed portion far away from the fracture surface in the CA specimens. It is seen in Fig. 9a (arrow) that a crack is formed at the centre region of the grain boundary which inclines to the tensile axis. Two types of grain boundary cracking are observed in Fig. 9b: one (A) is the type that the slid grain boundary itself fractures – this is thought to be the same type as in Fig. 9a but with further developed cracking; the other (B) is a wedge-type cracking formed by sliding of neighbouring grain boundaries, i.e. this is the same type that Chang and Grant have observed in creep deformation of a coarse grained Al–20%Zn alloy [18]. The arrow shows necking formed at the portion near a triple

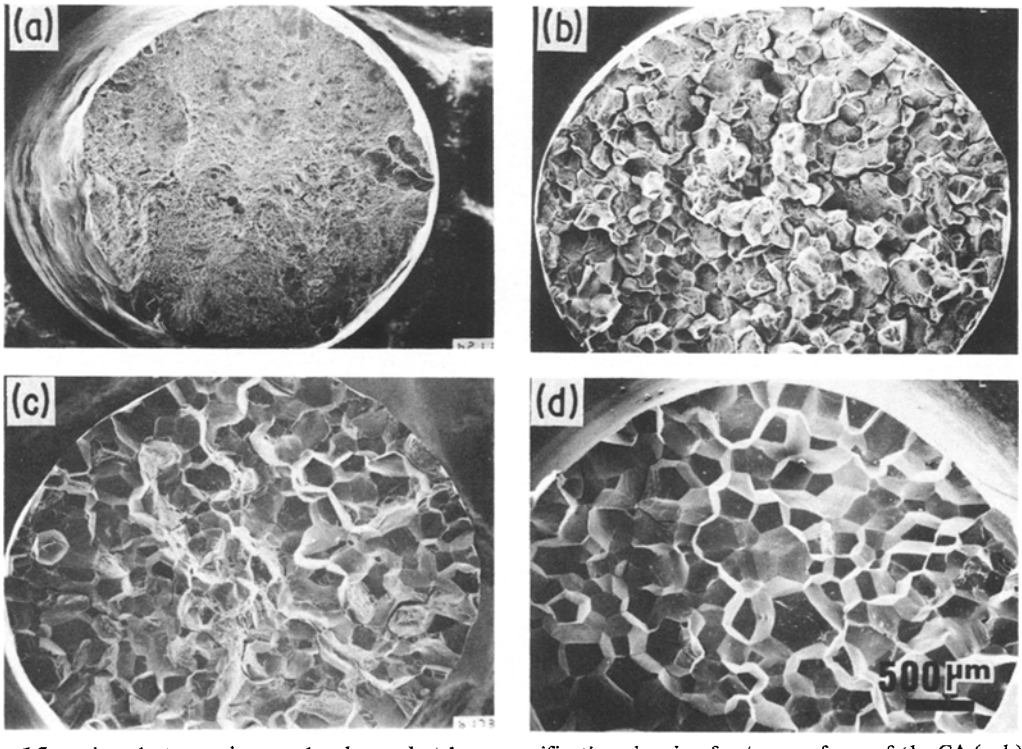

Figure 5 Scanning electron micrographs observed at low magnification showing fracture surfaces of the CA (a, b), and the A specimen (c, d), tested at 293 ((a) and (c)), and 4.2 K ((b) and (d)).

TABLE III Area fractions of transgranular fracture (%)

Temperature (K)	Cold working and ageing	Ageing only
293	96.0	20.4
196	94.2	2.8
77	36.9	1.1
4.2	29.7	1.1

point and at the ends of the grain boundary cracking. Fig. 9c shows an example of grain boundary cracking at the uniformly deformed portion far away from the fracture surface in the A specimen. Similar to the CA specimen, it is characteristic that cracking occurs at the centre portion of the grain boundary inclined about 45° to the tensile axis. Fig. 9d shows an optical micrograph of the shear fracture region on the longitudinal section of the CA specimen tested at 293 K.

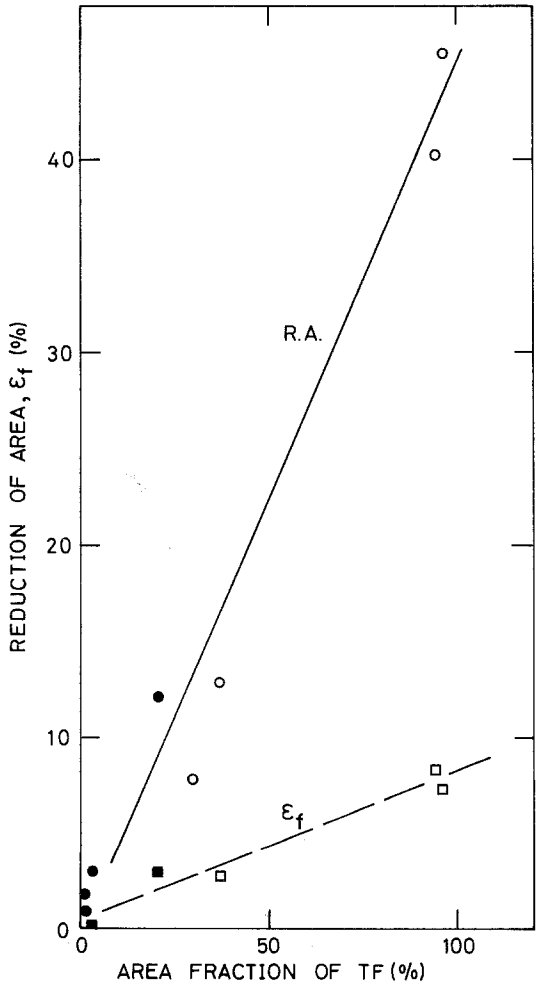

Figure 6 Relationships between the area fraction of transgranular fracture and the fracture strain and the reduction of area.

Large and wavy transgranular cracks are observable in the heavily sheared region.

4. Discussion

4.1. An outline of two types of intergranular fracture in Al–Zn–Mg alloys

In age hardenable Al–Zn–Mg alloys two types of intergranular fracture, i.e. the ledge- and the dimple-formation type have been known. Little information has been gained on the intergranular fracture of the ledge-formation type [5, 6]. On the other hand many investigators have reported evidence of dimples formed on the intergranular fracture surfaces [1–4, 16]. Kawabata and Izumi [2] pointed out that the shear deformation in PFZ plays an important role in the intergranular fracture of the dimple-formation type [2].

Figs. 10a and b show schematic drawings for explaining the intergranular fracture of the ledge- and the dimple-formation type. In the ledge-formation type, the interaction between grain boundaries and dislocations forms grain boundary cracks at the front of slip bands. In this case PFZ would act to relax the stress concentration of the slip bands, as pointed out by Ryum [19]. It is the dimple-formation type that the fracture of grain boundary precipitates themselves or the separation of the interface of grain boundary precipitates due to the strong shear deformation along the grain boundary in PFZ provides the nuclei of voids, and the growth and the coalescence of voids by the subsequent shear deformation results in a macroscopic crack. Also in this type, as shown in the Equation 31 of [2] with increasing the width of PFZ the alloy becomes more ductile if the mean size and the number of grain boundary precipitates per unit area are not changed.

4.2. On the cause of the reduction of intergranular fracture by the CA treatment

Fig. 11 is a schematic drawing showing the grain boundary morphology and the existence of subboundaries in the CA specimens. The grain boundaries of the CA specimen run in a zigzag way as shown in Figs. 2b and c. Therefore, the shear deformation along the grain boundary in PFZ is disturbed by the steps on the boundary (e.g. at A and B in Fig. 11). It corresponds to the shortening of the grain boundaries or to a smaller grain size. That is, the dimple-formation type intergranular

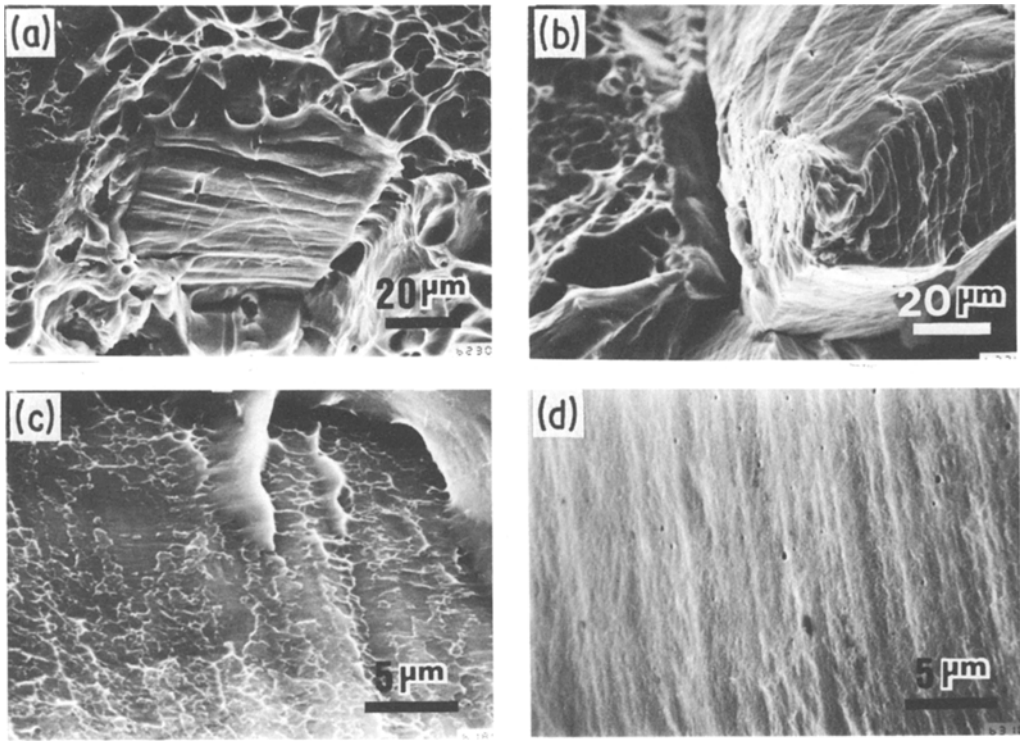

Figure 7 Scanning electron micrographs observed at high magnification showing the intergranular fracture surfaces of the CA ((a) and (b)) and the A specimen ((c) and (d)) tested at 293 ((a) and (c)), 196 (d) and 4.2 K (b).

fracture in the CA specimen will initiate at the later stage of deformation than in the A specimen. However, in the case where the steps are formed in the opposite direction to the shear the steps may supply the origin of intergranular fracture (e.g. at B in Fig. 11). This will be discussed in Section 4.3.

Next, we will consider the parameters relating the ledge-formation type intergranular fracture. In Fig. 2 we saw the dense subboundaries in grains and a large number of precipitates on the subboundaries in the CA specimen. These suppress the development of slip bands and reduce the

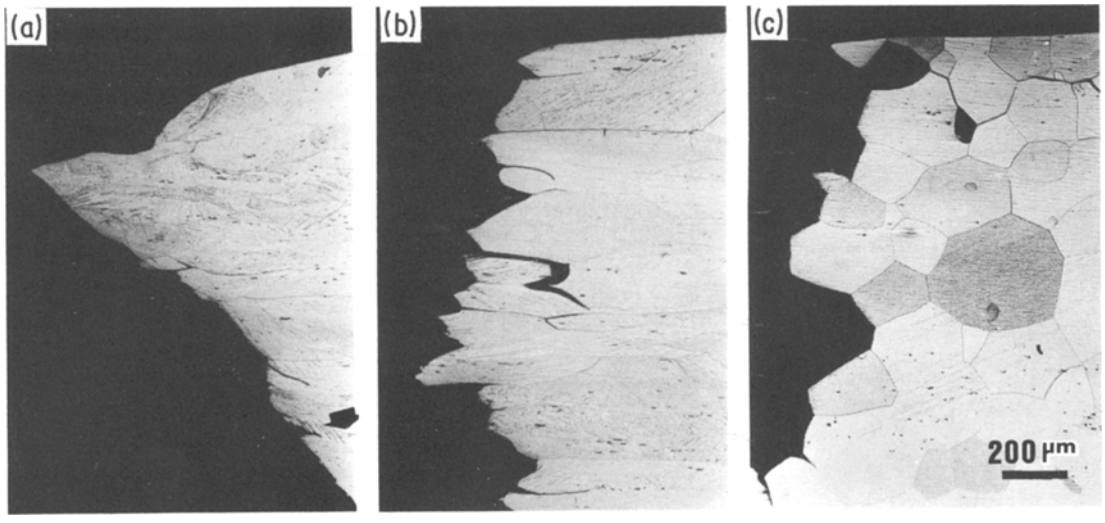

Figure 8 Optical micrographs showing the longitudinal section near the fracture portion of the CA ((a) and (b)) and the A specimen (c) tested at 196 ((a) and (c)) and 77 K (b). The arrows shows the end of the grain boundary cracking along tensile axis formed at a region far away from the fractured portion.

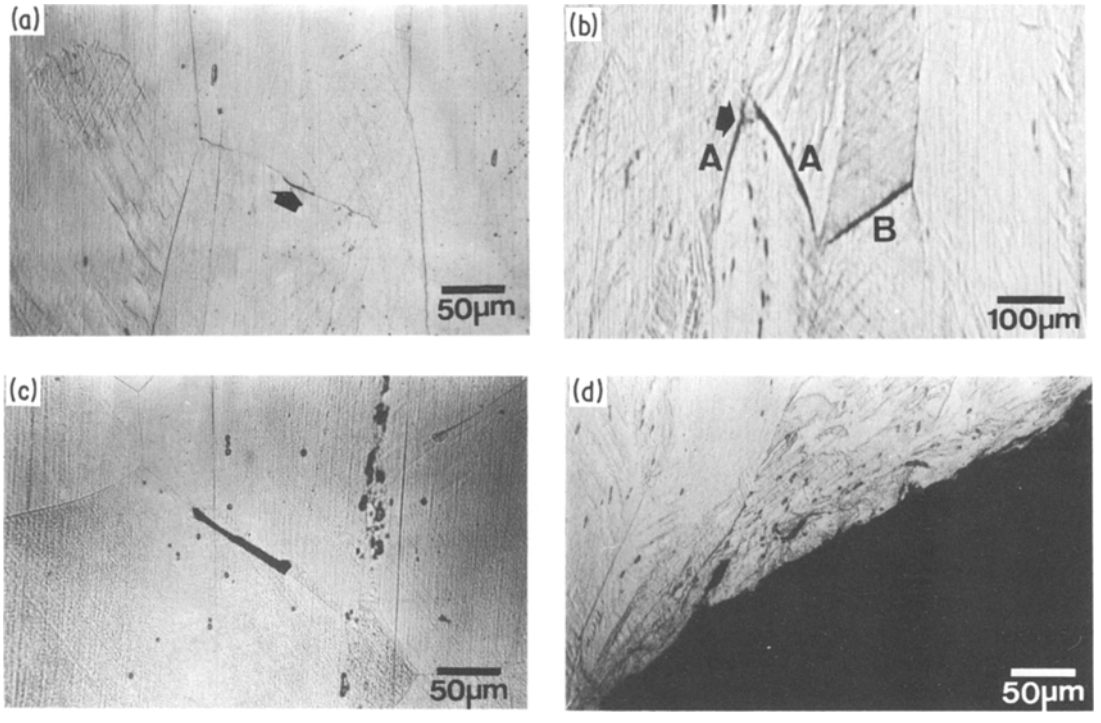

Figure 9 Optical micrographs showing the intergranular cracking ((a) to (c)) and the large voids at the shear region in a grain (d), in the CA (a, b and d) and the A specimen (c).

occurrence of the intergranular fracture due to the ledge formation because the subboundaries and the precipitates act as obstacles against the movement of dislocations.

In addition, there are dense dislocations in the CA specimen which were produced by cold working after solution treatment and remain even after ageing treatment. The dense dislocations provide a large number of dislocation sources so that they bring the more uniform deformation in grains. Moreover there are various sizes of precipitate in the matrix (see Table I). This also strengthens the tendency to deform uniformly because it is difficult for the dislocations to cut the large precipitates. Such uniform deformation reduces the tendency of intergranular fracture due to the ledge formation.

As described above, in the CA specimens each parameter, such as the shape of grains, the existence of subboundaries, the size distribution of precipi-

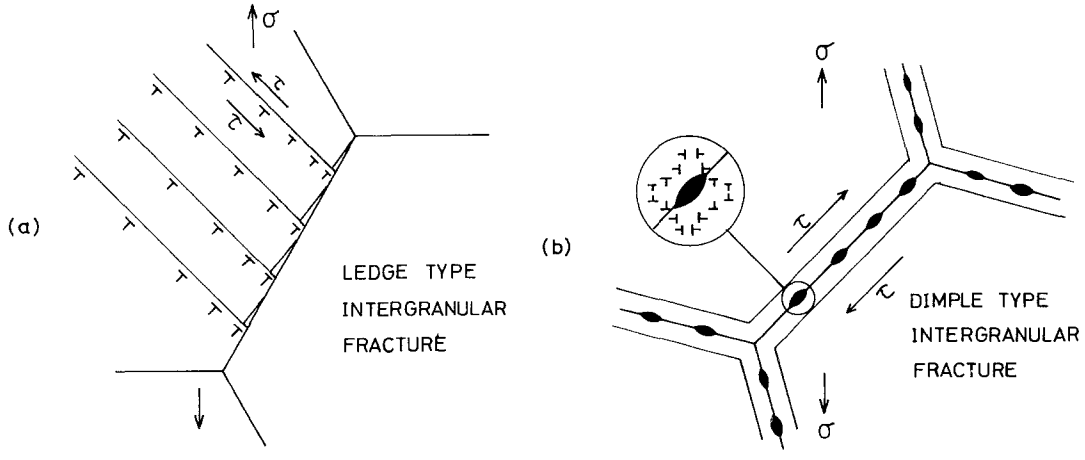

Figure 10 Schematic representations of the ledge (a), and the dimple-formation type intergranular fracture (b).

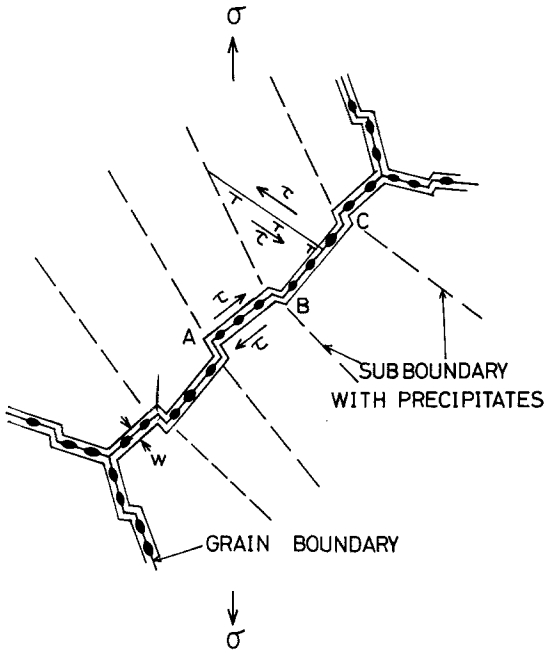

Figure 11 A schematic representation of the cause increasing ductility in relation to two types of intergranular fracture mechanism.

tates in grains, and a large number of dislocations remaining in grains suppresses both types of intergranular fracture mechanism and as a result ductility increases.

4.3. The mechanism of intergranular fracture in the CA specimens

As shown in Figs. 9a and b the intergranular fracture in the CA specimen occurs on the grain boundaries inclined about 45° to tensile axis. The PFZ is more deformable than in grains with precipitates so that the shearing deformation will concentrate in the PFZ. According to the observation of fracture surfaces (Figs. 7a to c) the intergranular fracture of the CA specimens is not due to the dimple-formation type but due to the ledge-formation type. These results would show that the shear deformation in PFZ along grain boundaries also plays an important role in the ledge-formation type intergranular fracture due to slip bands in grains.

Fig. 12 shows schematic drawings explaining the occurrence of cracks of the ledge-formation type by both the grain boundary sliding (or the shear deformation in PFZ) and the slip bands in grains. Now, in Fig. 12a when the shear stress τ acts along grain boundary ABC, grain boundary sliding will be obstructed at the steps A and C, but yield a gap at the step B, especially at the higher strain (Fig. 12b). Dislocations at the fronts of slip band will be absorbed into the gap, resulting in the formation of the ledge-formation type intergranular fracture as shown in Fig. 12c.

4.4. Estimation of the intergranular fracture stress in the CA specimen

The CA specimens fractured intergranularly by a ledge formation type and not by a dimple formation type. Now, we will estimate the intergranular fracture stresses of both types and show that the ledge formation type, described in Section 4.3, will occur more favourably than the dimple formation type, by comparing the fracture stresses.

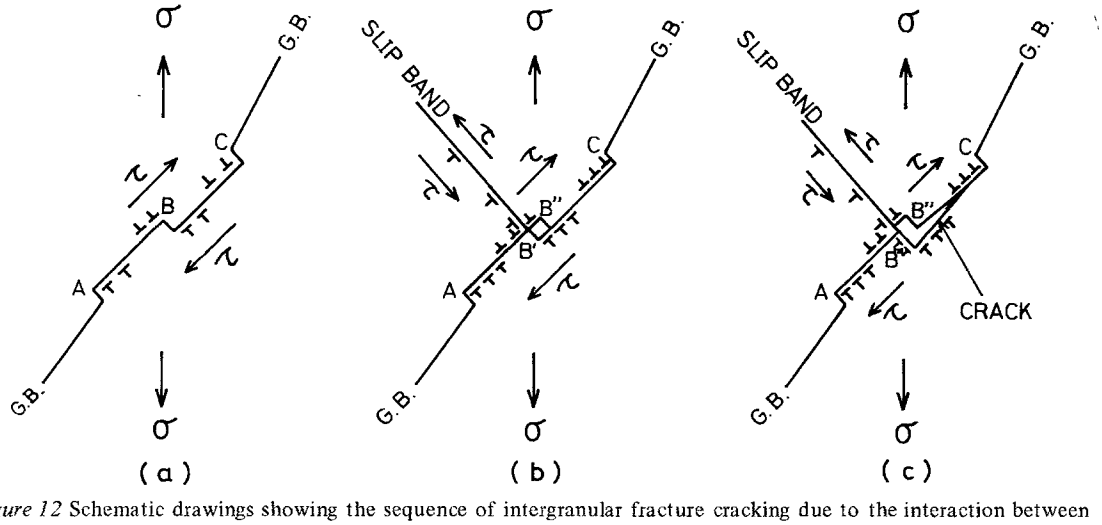

Figure 12 Schematic drawings showing the sequence of intergranular fracture cracking due to the interaction between shearing deformation along PFZ and dislocations within the matrix in an Al–Zn–Mg alloy applied the cold working and ageing treatment.

4.4.1. The intergranular fracture stress of the dimple formation type

Many steps, which were observable in the transmission electron micrograph and also on the fracture surfaces of the CA specimen, may act as an obstacle to shearing deformation within PFZ along grain boundaries. However, the shearing deformation will occur in the PFZ between steps, similarly as in grain boundaries without steps, so that the CA specimen has the possibility of fracturing by the dimple formation type for the shearing deformation.

We suppose the following situation; a dislocation source exists in the PFZ at the middle of a grain boundary between steps; a group of piled up dislocations is formed within PFZ and in matrix with precipitates on the extension of the PFZ by the applied shear stress, τ; the shear strain γ_m occurs in PFZ between steps due to growth of the dislocation piling up; when γ_m reaches a given critical value γ_f, a macroscopic crack is formed by a mechanism of void nucleation, growth and coalescence; then τ gives the intergranular fracture stress of dimple-formation type, $\tau_{f,d}$. Now, we get a relationship between $\tau_{f,d}$ and γ_f as follows (see Appendix I).

$$\tau_{f,d} = \tau_{i,m} - \frac{\alpha^2 a}{\beta + \alpha a} \quad (1)$$

$$\alpha = \tau_{i,m} - \tau_{i,PFZ} \quad (2)$$

$$\beta = \frac{G}{\pi(1-\nu)} w\gamma_f, \quad (3)$$

where $\tau_{i,m}$ and $\tau_{i,PFZ}$ are the internal stress against the movement of dislocations in the matrix with precipitates and in PFZ, respectively, a the average length of grain boundary between steps, w the width of PFZ, G the shear modulus, ν the Poisson's ratio. $\tau_{i,m}$, $\tau_{i,PFZ}$, w and γ_f* are changeable by heat treatment, but they are considered to be constants in the same alloy and under the same heat treatment. a is also changeable by cold working.

4.4.2. The intergranular fracture stress of the ledge-formation type in the CA specimen

When cracking occurs at the steps of grain boundary $\tau_{f,1}$, which is the intergranular fracture stress of ledge-formation type, is given by

$$\tau_{f,1} = \tau_{i,PFZ} + k_f a^{-1/2} \quad (4)$$

where

$$k_f = \left[2.24 \frac{\alpha' \mathbf{b} G^2}{\pi(1-\nu)}\right]^{1/2} \quad (5)$$

α' is 0.0495 for fcc alloys [6] and $\mathbf{b}$ is Burgers vector.

4.4.3. Comparison between the intergranular fracture stresses of the dimple-formation and the ledge-formation type

Now, we assume that $\tau_{i,m}$ and $\tau_{i,PFZ}$ are 254 and 132 MPa, which are halves of the ultimate tensile stress in the aged CA and the as-quenched specimens, respectively. a is about 3.5×10^{-6} m from the observations of fracture surfaces and of transmission electron micrographs. w is about 2×10^{-8} m from the observation of transmission electron micrographs, and $G = 2.45 \times 10^4$ MPa, $b = 2.86 \times 10^{-10}$ m and $\nu = 0.33$ [20]. And we also assume as $\gamma_f \simeq 10$. Then, putting the above values into Equations 1 and 4 we obtain $\tau_{f,d} = 235$ and $\tau_{f,1} = 182$ MPa, repsectively. From $\tau_{f,d} > \tau_{f,1}$, it is concluded that in the present alloy the intergranular fracture of the ledge-formation type is more favourable than that of the dimple-formation type. The above calculation coincides with the experimental results that the CA specimens fracture mainly by the ledge-formation type.

4.5. On the lowering of ductility with decreasing temperature

With decreasing testing temperature, the ductility and the area fraction of intergranular fracture are lowered even in the CA specimens.

Now we consider the change of the strain concentration to PFZ with decreasing temperature. The strain concentration to PFZ will depend on the difference between resistances against the movement of dislocations, or flow stress, in matrix and in PFZ. That is, the greater $(\Delta\sigma)_T$, in the following equation, brings the larger strain concentration into PFZ.

$$(\Delta\sigma)_T = (\sigma_m)_T - (\sigma_{PFZ})_T \quad (6)$$

Where, $\Delta\sigma$ is the difference between resistances against the movement of dislocations in the matrix, σ_m, and in the PFZ, σ_{PFZ}, at the temperature, T.

*γ_f will depend upon the average size and the density of grain boundary precipitates, and the width of PFZ [2]. Therefore, γ_f is considered to be a constant under the same heat treatment.

TABLE IV Differences between yield stresses in an Al–6.0 % Zn–2.6 % Mg alloy applied the cold working and ageing treatment (the present work) and in an Al–4.7 % Zn–1.26 % Mg alloy as-quenched [24] at 293, 196 and 77 K

Temperature (K)	Yield stress, $\sigma_{0.2}$ (MPa)		Difference, $\Delta\sigma_{0.2}$ (MPa)
	Al–6.0 % Zn–2.6 % Mg alloy cold worked and aged (present work)	Al–4.7 % Zn–1.26 % Mg alloy as-quenched [24]	
293	473	77	396
196	497	90	407
77	588	104	484

For simplification, we will assume that

$$\sigma_m \simeq \sigma_{0.2,a} \quad \text{and} \quad \sigma_{PFZ} \simeq \sigma_{0.2,q},$$

i.e. $(\Delta\sigma)_T \simeq (\sigma_{0.2,a})_T - (\sigma_{0.2,q})_T$, where $\sigma_{0.2,a}$ and $\sigma_{0.2,q}$ represent the 0.2% proof stresses in the aged and in the as-quenched condition, respectively.

The content of solute atom in PFZ is variable with ageing condition [21]. When aged at 393 K for 86.4 ksec in the present study, the content of zinc and magnesium in the PFZ would be reduced to a given amount from the average content. According to Kovács *et al.* the values of $\sigma_{0.2}$ at 293, 196 and 77 K in an Al–4.7 % Zn–1.26 % Mg alloy after solution treatment and ageing at room temperature for 180 sec (which corresponds to the as-quenched condition) are 77, 90 and 104 MPa, respectively [22]. Therefore, the values of $\Delta\sigma$ at 293, 196 and 77 K obtained from the results by Kovács *et al.* and by the present study are 396, 407 and 484 MPa, respectively (Table IV). The value of $\Delta\sigma$ increases with decreasing temperature. That is, the decrease of temperature brings the strain concentration into PFZ, and subsequently the pronounced tendency of the intergranular fracture.

As other causes of lowering ductility with decreasing temperature, it should be considered that the decrease of temperature makes it easy to fracture the grain boundary precipitates themselves.

5. Conclusions

The effect of cold working and ageing treatment (CA) on the mechanical properties at 4.2 to 293 K and the ductility improvement mechanism due to the CA treatment in an Al–6.0 % Zn–2.6 % Mg alloy were investigated. The CA treatment improved the ductility of the alloy at cryogenic temperatures. It was found that both the fracture strain and the reduction of area (RA) varied linearly with the area fraction of transgranular fracture. The ductility improvement by the CA treatment is thought to be due to the suppression of both the ledge- and the dimple-formation type intergranular fracture because of the zigzag grain boundaries, the formation of a large number of subboundaries in grains and the scattering precipitate size. However, the trend of intergranular fracture is pronounced with decreasing temperature and this may be due to the increased difference between flow stresses in PFZ and matrix and the embrittlement of grain boundary precipitates at low temperatures. The intergranular fracture in the CA specimens would be attributed to the interaction between the grain boundary sliding and the slip bands in grains.

Acknowledgement

This work was supported partly by the Keikinzoku Shogakukai (The Light Metal Educational Foundation, Incorporated).

Appendix I The intergranular fracture stress of dimple-formation type in the CA specimen

A large number of steps were seen on grain boundaries in the transmission electron micrographs in the CA specimens. The steps become a strong resistance against the shear deformation in PFZ along grain boundaries. Therefore, it is hard to cause the intergranular fracture of dimple-formation type due to the shear deformation within the PFZ. However, when an applied stress operates along a grain boundary with steps, as shown in Fig. A1a, the shear deformation will propagate from the interior of PFZ into a matrix with precipitates on the extension of PFZ (e.g. as C → X, D → Y). The propagation strengthens the shear deformation within PFZ so that the intergranular fracture of dimple-deformation type may occur between steps. During development of the deformation band, cracks may be formed at the corners B and C of grain boundary, and then the combination of both cracks makes a gap at the step. It has been described in Section 4.3 that one kind of

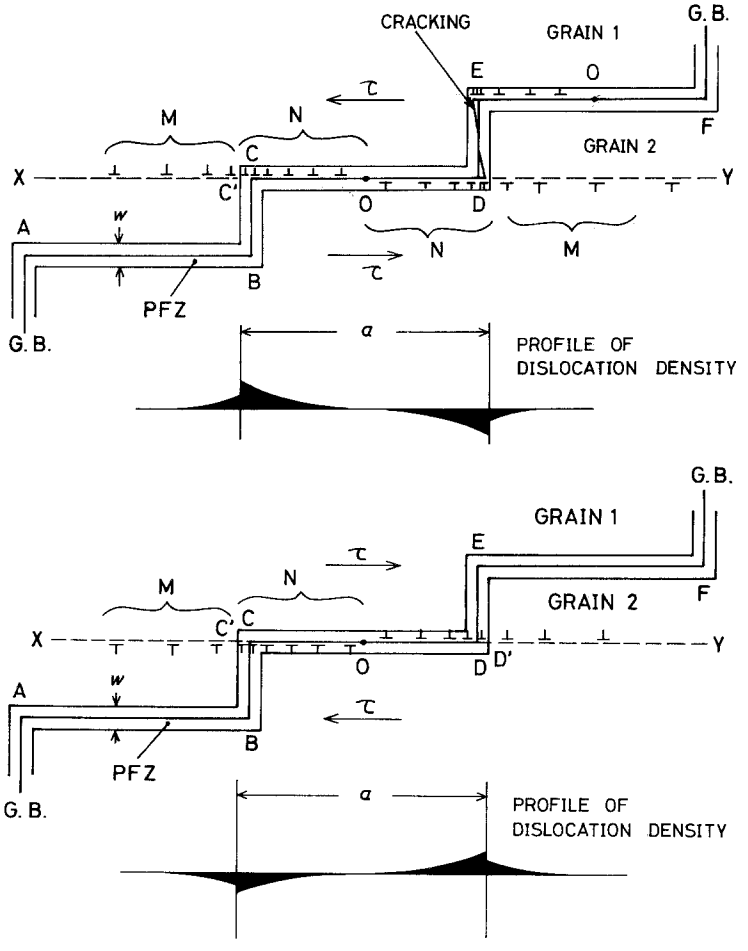

Figure A1 Schematic drawings showing deformation in the PFZ and in the extension of PFZ. Cracking can nucleate in (a) but cannot nucleate in (b). At the lower portion in (a) and (b) the profiles of dislocation density are shown.

the intergranular fracture of ledge-formation type occurs due to the absorption of dislocations into the gap. Then the fracture stress was estimated in Section 4.4.3. At the lower portion in Fig. A1a a profile of dislocation density is shown.

Fig. A1b shows the case for the applied shear stress acting in the opposite direction against the above. In this case no crack is formed at the steps but only a deformation band will develop in PFZ and on the extension of PFZ, because the applied shear stress always works in the direction closing the crack.

Even though a force applied to dislocations and position of dislocations are calculated statically or dynamically, both calculations will not bring so large difference. Therefore we will treat statically the pile up of dislocations.

Now, three cases are considered as to the relative magnitude of the applied shear stress, τ, and the internal stresses in the matrix with precipitates, $\tau_{i,m}$, and in the PFZ, τ_i,

$$\tau_{i,m} > \tau_{i,PFZ} > \tau \quad \text{(A1)}$$

$$\tau_{i,m} > \tau > \tau_{i,PFZ} \quad \text{(A2)}$$

$$\tau > \tau_{i,m} > \tau_{i,PFZ} \quad \text{(A3)}$$

In the case of Equation A1 no dislocation acts in the whole specimen. In the case of Equation A2, the deformation occurs at first only within the PFZ and, at the latter stage, propagates to the region with precipitates on the extension of the PFZ. In the case of Equation A3 dislocations act not only in the PFZ but also in the whole specimen. Also in this case it is inevitable that the deformation concentrates to the PFZ and on the extension of the PFZ. At the higher stress level than in the case of Equation A2, namely the case of Equation A3 should be regarded as the uniform deformation added the concentrated deformation within the PFZ and the extension of the PFZ.

The effective stresses in the matrix, $\tau_{e,m}$, and in the PFZ, $\tau_{e,PFZ}$, are

$$\tau_{e,PFZ} = \tau - \tau_{i,PFZ} > 0 \quad \text{(A4)}$$

$$\tau_{e,m} = \tau - \tau_{i,m} < 0 \quad \text{(A5)}$$

under the condition of $\tau_{i,m} > \tau > \tau_{i,PFZ}$. In Fig. A1a, it is assumed that there exists a dislocation source at the centre, O, of a part of grain boundary, CD, and the piling up of dislocations within the PFZ is developed by multiplication of dislocation from the source. By increasing the applied stress the dislocations within the PFZ will push out to the extension of the PFZ and a piled up dislocation group of XCO will be formed. (When the piling-ups of dislocations are formed on some slip planes they can be approximately replaced to a piling up of dislocations on one slip plane [23].) The force on the last dislocation pushed out from PFZ to grain interior, τ_c, is expressed by the stress at the point C on the edge of the PFZ. For simplification, the stress is assumed as a short range stress acting only the Mth dislocations. Then the equilibrium equation of the Mth dislocation becomes as follows.

$$\sum_{j=1}^{M-1} \frac{A}{x_j - x_M} + (\tau - \tau_{i,m}) = \tau_c \quad \text{(A6)}$$

where x_M and x_j are the positions of dislocations from the point C, and

$$A = \frac{Gb}{2\pi(1-\nu)} \quad \text{(A7)}$$

The equilibrium equation for the ith dislocation is expressed as*

$$\sum_{\substack{j=1 \\ j=i}}^{M} \frac{A}{x_j - x_i} + (\tau - \tau_{i,m}) = 0 \quad \text{(A8)}$$

The action force is equal to the reaction one. By considering inversely the action and the reaction force, the meaning of Equation A8 is changeable as M dislocations piling up from X to C under the effective stress $(\tau_{i,m} - \tau)$. Therefore, the solution of Cottrell [24] and Eshelby [25] can be also used to the piling up dislocations described above. That is, the stress acting to the Mth dislocation, τ_c, is obtained as

$$\tau_c = M(\tau_{i,m} - \tau) \quad \text{(A9)}$$

The τ_c is created also by the piled up dislocations in the PFZ along OC, therefore,

$$\tau_c = N(\tau - \tau_{i,PFZ}) \quad \text{(A12)}$$

Here, when the grain boundary length between the steps is a, the number of the piled up dislocations in the PFZ, N, is expressed as follows [23]

$$N = \frac{a(\tau - \tau_{i,PFZ})}{4A} \quad \text{(A13)}$$

From Equations A9, A12 and A13,

$$M = \frac{a(\tau - \tau_{i,PFZ})^2}{4A(\tau_{i,m} - \tau)} \quad \text{(A14)}$$

The M dislocations have the piled up length L ($< d$, the grain size) on the slip plane CX, so Equation A14 is also expressed as

$$M = \frac{L(\tau_{i,m} - \tau)}{2A} \quad \text{(A15)}$$

The relative shearing displacements at the end point C of PFZ, S_c, and the additional shearing displacement at the central point O between the steps C and D, S_{oa}, are

$$S_c = Mb = \frac{a(\tau - \tau_{i,PFZ})^2}{4A(\tau_{i,m} - \tau)} b \quad \text{(A16)}$$

$$S_{oa} = Nb = \frac{a(\tau - \tau_{i,PFZ})}{4A} b \quad \text{(A17)}$$

The total relative displacement at the point O, S_m, is two times the summation of both, i.e.

$$S_m = \frac{\xi}{\tau_{i,m} - \tau} - \eta \quad \text{(A18)}$$

where

*For simplification, we assume, now, that the groups of dislocations in the grain and the PFZ interact only through the Mth and lth dislocation. But actually we should consider the interaction regarding the dislocation groups in the grain and in the PFZ as one group of dislocations. Then the equilibrium equation of the ith dislocation is a little different by the position of the ith dislocation being within the grain or in the PFZ, that is,

$$\sum_{\substack{j=1 \\ j\neq i}}^{M+N} \frac{A}{x_j - x_i} + (\tau - \tau_{i,m}) = 0 \quad \text{(in grain)} \quad \text{(A10)}$$

or

$$\sum_{\substack{j=1 \\ j\neq i}}^{M+N} \frac{A}{x_j - x_i} + (\tau - \tau_{i,PFZ}) = 0 \quad \text{(in PFZ)} \quad \text{(A11)}$$

respectively.

$$\xi = \frac{\pi(1-\nu)}{G} a(\tau_{i,m} - \tau_{i,PFZ})^2 \quad \text{(A19)}$$

$$\eta = \frac{\pi(1-\nu)}{G} a(\tau_{i,m} - \tau_{i,PFZ}) \quad \text{(A20)}$$

a is changeable by cold working, and $\tau_{i,PFZ}$ and $\tau_{i,m}$ are also changeable a little and largely by heat treatment, respectively. Therefore, ξ and η are considered to be constants in the same alloy and in the same heat treatment.

From an idea that S_m occurs due to the uniform shearing strain in PFZ, γ_m, we can replace S_m with γ_m.

$$S_m = w\gamma_m \quad \text{(A21)}$$

where w is the width of PFZ.

Now, we assume that a grain boundary cracking with a macroscopic size occurs when γ_m reaches a critical value γ_f at the central portion between the steps. Then the intergranular fracture stress of the dimple-formation type, $\tau_{f,d}$, in the CA specimen due to the shearing deformation within PFZ is expressed as follows

$$\tau_{f,d} = \tau_{i,m} - \frac{a(\tau_{i,m} - \tau_{i,PFZ})^2}{\frac{G}{\pi(1-\nu)} w\gamma_f + a(\tau_{i,m} - \tau_{i,PFZ})} \quad \text{(A22)}$$

For the A specimens, the fracture stress of dimple-formation type, $\tau'_{f,d}$ can be represented by the same Equation A22 by replacing a with the length of grain boundary side a'.

References

1. D. A. RYDER and A. C. SMALE, "Fracture of Solids", edited by D. C. Drucker and J. J. Gilman (Interscience, New York, 1963) p. 237.
2. T. KAWABATA and O. IZUMI, *Acta Metall.* **24** (1976) 817.
3. A. J. SEDRIKS, P. W. SLATTERY and E. N. PUGH, *Trans. ASM* **62** (1969) 238, 815.
4. P. N. T. UNWIN and G. C. SMITH, *J. Inst. Met.* **97** (1969) 299.
5. N. RYUM and K. BAARDETH, *ibid.* **96** (1968) 92.
6. T. KAWABATA and O. IZUMI, *J. Mater. Sci.* **14** (1979) 1071.
7. J. L. CHRISTIAN and J. F. WATSON, *Adv. Cryogenic Eng.* **6** (1961) 604.
8. J. G. KAUFMAN, K. O. BOGARDUS and E. T. WANDERER, *ibid.* **13** (1967) 294.
9. J. G. KAUFMAN and E. T. WANDERER, *ibid.* **16** (1970) 27.
10. E. DiRUSSO, M. CONSERVA, F. GATTO and H. MARKUS, *Metall. Trans.* **4** (1973) 1133.
11. E. DiRUSSO, M. CONSERVA, M. BURATTI and F. GATTO, *Mater. Sci. Eng.* **14** (1974) 23.
12. T. F. BOWER, S. N. SINGH and M. C. FLEMINGS, *Metall. Trans.* **1** (1970) 191.
13. J. WALDMAN, H. SULINSKI and H. MARKUS, *ibid.* **5** (1974) 573.
14. J. MERCIER and R. CHEVIGNY, *Mem. Sci. Rev. Met.* **60** (1963) 61.
15. D. S. THOMPSON, S. A. LEVY and G. E. SPANGLER, *Aluminium* **50** (1974) 647.
16. T. UNO and Y. BABA, *J. Jpn. Inst. Met.* **42** (1978) 388.
17. P. N. T. UNWIN and R. B. NICHOLSON, *Acta Metall.* **17** (1969) 1379.
18. H. C. CHANG and N. J. GRANT, *J. Met.* **8** (1956) 544.
19. N. RYUM, *Acta Metall.* **16** (1968) 327.
20. L. F. MONDOLFO, "The Aluminium–Magnesium–Zinc Alloys", Research and Development Center, Revere Copper and Brass Incorporated, Rome, New York, 1967, p. 171.
21. P. DOIG, J. W. EDINGTON and G. HIBBERT, *Phil. Mag.* **28** (1973) 971.
22. I. KOVACS, J. LENDVAI, T. UNGER, G. GROMA and J. LAKNER, *Acta Metall.* **28** (1980) 1621.
23. A. N. STROH, *Proc. Roy. Soc.* **A232** (1955) 548.
24. A. H. COTTRELL, "Dislocations and Plastic Flow in Crystals" (Oxford University Press, Oxford, 1965) p. 104.
25. J. D. ESHELBY, F. C. FRANK and F. R. N. NABARRO, *Phil. Mag.* **42** (1951) 351.

Received 14 February
and accepted 26 July 1983